*Inorg. Chem.* **2006**, *45*, 7689–7697


# Dimethylammonium Trichlorocuprate(II): Structural Transition, Low-Temperature Crystal Structure, and Unusual Two-Magnetic Chain Structure Dictated by Nonbonding Chloride–Chloride Contacts

**Roger D. Willett***

*Department of Chemistry, Washington State University, Pullman, Washington 99164*

**Brendan Twamley**

*University Research Office, University of Idaho, Moscow, Idaho 83844*

**Wouter Montfrooij,[†] Garrett E. Granroth, and Stephen E. Nagler**

*Oak Ridge National Laboratory, Oak Ridge, Tennessee 37831*

**Donavan W. Hall[‡]**

*National High Magnetic Field Laboratory, Florida State University, Tallahassee, Florida 32210*

**Ju-Hyun Park, Brian C. Watson,[§] and Mark W. Meisel**

*Department of Physics, University of Florida, Gainesville, Florida 32611-8440*

**Daniel R. Talham***

*Department of Chemistry, University of Florida, Gainesville, Florida 32611-7200*

Received April 17, 2006

Catena(dimethylammonium-bis($\mu_2$-chloro)-chlorocuprate), $(CH_3)_2NH_2CuCl_3$, forms chains of $Cu_2Cl_6^{2-}$ bifold dimers linked along the structural chain axis by terminal chlorides forming long semicoordinate bonds to adjacent dimers. The structural chains are separated by dimethylammonium ions that hydrogen bond to chloride ions of the dimers. A structural phase transition below room temperature removes disorder in the hydrogen bonding, leaving adjacent dimers along the chain structurally and magnetically inequivalent, with alternating ferromagnetic and antiferromagnetic pairs. The coupled dimers are magnetically isolated from each other along the structural chain axis by the long semicoordinate Cu–Cl bond. However, the dimers couple to like counterparts on adjacent chains via nonbonding Cl···Cl contacts. The result is two independent magnetic chains, one an alternating antiferromagnetic chain and the other an antiferromagnetic chain of ferromagnetically coupled copper dimers, which run perpendicular to the structural chains. This magnetostructural analysis is used to fit unusual low-temperature (1.6 K) magnetization vs field data that display a two-step saturation. The structural phase transition is identified with neutron scattering and capacitance measurements, and the X-ray crystal structures are determined at room temperature and 84 K. The results appear to resolve long-standing confusion about the origins of the magnetic behavior of this compound and provide a compelling example of the importance of two-halide magnetic exchange.

## Introduction

Molecule-based magnetism provides a platform to study a wide range of novel magnetic behavior drawing the attention of both experimentalists and theorists. Alkylammonium copper halides constitute one of the oldest and best-studied families of molecule-based magnets, providing multiple important examples of dimers,[1−5] chains,[6−10] ladders,[11−14] and two-dimensional sheets[15−21] for discerning detailed structure/property relationships. One of the note-

* To whom correspondence should be addressed. Email: rdw@mail.wsu.edu (R.D.W.); talham@chem.ufl.edu (D.R.T.).

[†] Present address: Department of Physics and Astronomy, University of Missouri, Columbia, MO 65211.

[‡] Present address: PRL Editorial Offices, One Research Road, Box 9000, Ridge, NY 11961-9000.

[§] Present Address: Information Systems Laboratories, Inc., San Diego, CA 92121.

(1) Roundhill, S. G. N.; Roundhill, D. M.; Bloomquist, D. R.; Landee, C.; Willett, R. D.; Dooley, D. M.; Gray, H. B. *Inorg. Chem.* **1979**, *18*, 831.

10.1021/ic060654u CCC: $33.50 
Published on Web 08/18/2006

worthy but often overlooked lessons of copper halide extended systems is the importance of magnetic exchange via nonbonding halide−halide contacts, sometimes called two-halide exchange[5] or super-superexchange,[22,23] that can lead to magnetic interactions that are equal to or stronger than those mediated by covalent superexchange pathways.[3,5,17,19,20,22,24,25] The title compound provides an elegant example of how this overlooked interaction is responsible for otherwise confusing magnetic behavior.

The structure of $(CH_3)_2NH_2CuCl_3$ was reported in 1966[26] and contains $Cu_2Cl_6^{2-}$ dimers linked by pairs of semicoordinate Cu···Cl bonds to form linear chains separated by the dimethylammonium ions. The metal ion coordination is the folded 4 + 1 geometry common for copper(II) ions. Several studies of the magnetic and thermodynamic properties were subsequently reported.[4,27−29] In the earliest study of the low-temperature magnetic susceptibility, deviations from Curie−Weiss behavior were observed below 10 K[29] for a powder sample and attributed to antiferromagnetic interactions. The low-temperature (1.2−28.6 K) specific heat was investigated by Hurley and Gerstein,[28] and after subtracting the lattice contribution, the temperature dependence of the magnetic specific heat had a form that is often observed in low-dimensional systems. Assuming the dimers were ferromagnetically coupled, the data were fit with an $S = 1$ Heisenberg (chain) antiferromagnet model that yielded an interdimer coupling constant $J/k_B = -4.92$ K.[28]

In 1988, O'Brien et al.[4] reported an unusual field dependence of the high-field (up to 30 T), low-temperature ($T = 1.2$ K) magnetization behavior that deviated significantly from that expected for a linear chain of antiferromagnetically coupled $S = 1$ dimers. The prominent feature is an apparent two-step saturation of the magnetization for which a plateau corresponding to half-saturation is reached near 5 T, but full saturation is not achieved until 15 T. Current interest in integer spin chains has led to renewed attention for the low-temperature properties of $(CH_3)_2NH_2CuCl_3$, and this result has since been observed by other workers,[30−33] including the present study (vide infra).

Several groups have now extended these studies to lower temperatures, including measurements down to the millikelvin temperature range, and have expanded the probes to include inelastic neutron scattering. For example, Ajiro et al.[31] reported measurements of the low-field magnetic susceptibility from 2 to 300 K, specific heat from 0.5 to 20 K, and high-magnetic-field magnetization versus field data at temperatures between 0.5 and 4.2 K.[32] This group had the insight to realize that three different exchange pathways are required to explain the available data[33] and proposed alternating ferromagnetically and antiferromagnetically coupled dimers along the chain axis. In parallel, Stone and co-workers studied the low-field magnetic susceptibility and specific heat at low temperatures[34] while also performing inelastic neutron scattering experiments.[35] The data by Stone and co-workers show significant one-dimensional coupling, although not along the expected direction corresponding to the structural chain axis, but rather perpendicular to it.

It is clear that the room-temperature crystal structure consisting of a single chain of dimers cannot account for the unusual magnetic behavior seen at low temperatures. We therefore looked for evidence of a structural phase transition below room temperature, which we now report. The transition is observed below room temperature with neutron powder diffraction and confirmed near 287 K using capacitance techniques. An X-ray crystallographic structure determination at 84 K identifies the low-temperature phase. Apparent disorder in the cation network at high temperature is removed in the low-temperature structure, leading to


(2) Addison, A. W.; Landee, C. P.; Willett, R. D.; Wicholas, M. *Inorg. Chem.* **1980**, *19*, 1921.
(3) Marsh, W. E.; Hatfield, W. E.; Hodgson, D. J. *Inorg. Chem.* **1988**, *27*, 1819.
(4) O'Brien, S.; Gaura, R. M.; Landee, C. P.; Ramakhrishna, B. L.; Willett, R. D. *Inorg. Chim. Acta* **1988**, *141*, 83.
(5) Willett, R. D.; Butcher, R.; Landee, C. P.; Twamley, B. *Polyhedron* **2005**, *24*, 2222.
(6) Willett, R. D.; Landee, C. *J. Appl. Phys.* **1978**, *49*, 1329.
(7) Willett, R. D.; Landee, C. P.; Gaura, R. M.; Swank, D. D.; Groenendijk, H. A.; Vanduyneveldt, A. J. *J. Magn. Magn. Mater.* **1980**, *15*−*8*, 1055.
(8) Swank, D. D.; Landee, C. P.; Willett, R. D. *Phys. Rev. B* **1979**, *20*, 2154.
(9) Landee, C. P.; Wicholas, M.; Willett, R. D.; Wolford, T. *Inorg. Chem.* **1979**, *18*, 2317.
(10) Landee, C. P.; Willett, R. D. *Phys. Rev. Lett.* **1979**, *43*, 463.
(11) Watson, B. C.; Kotov, V. N.; Meisel, M. W.; Hall, D. W.; Granroth, G. E.; Montfrooij, W. T.; Nagler, S. E.; Jensen, D. A.; Backov, R.; Petruska, M. A.; Fanucci, G. E.; Talham, D. R. *Phys. Rev. Lett.* **2001**, *86*, 5168.
(12) Willett, R. D.; Galeriu, C.; Landee, C. P.; Turnbull, M. M.; Twamley, B. *Inorg. Chem.* **2004**, *43*, 3804.
(13) Giantsidis, J.; Turnbull, M. M.; Galeriu, C.; Landee, C. P.; Woodward, F. M. *Synth. Met.* **2001**, *122*, 517.
(14) Marsh, W. E.; Helms, J. H.; Hatfield, W. E.; Hodgson, D. J. *Inorg. Chim. Acta* **1988**, *150*, 35.
(15) Phelps, D. W.; Losee, D. B.; Hatfield, W. E.; Hodgson, D. J. *Inorg. Chem.* **1976**, *15*, 3147.
(16) Willett, R. D. *J. Chem. Phys.* **1964**, *41*, 2243.
(17) Block, R.; Jansen, L. *Phys. Rev. B* **1982**, *26*, 148.
(18) Halvorson, K.; Willett, R. D. *Acta Crystallogr. C* **1988**, *44*, 2071.
(19) Snively, L. O.; Haines, D. N.; Emerson, K.; Drumheller, J. E. *Phys. Rev. B* **1982**, *26*, 5245.
(20) Straatman, P.; Block, R.; Jansen, L. *Phys. Rev. B* **1984**, *29*, 1415.
(21) Woodward, F. M.; Landee, C. P.; Giantsidis, J.; Turnbull, M. M.; Richardson, C. *Inorg. Chim. Acta* **2001**, *324*, 324.
(22) Whangbo, M. H.; Koo, H. J.; Dai, D.; Jung, D. *Inorg. Chem.* **2003**, *42*, 3898.
(23) Whangbo, M. H.; Koo, H. J.; Dai, D. *J. Solid State Chem.* **2003**, *176*, 417.
(24) Deumal, M.; Landee, C. P.; Novoa, J. J.; Robb, M. A.; Turnbull, M. M. *Polyhedron* **2003**, *22*, 2235.
(25) Turnbull, M. M.; Landee, C. P.; Wells, B. M. *Coord. Chem. Rev.* **2005**, *249*, 2567.
(26) Willett, R. D. *J. Chem. Phys.* **1966**, *44*, 39.
(27) Lahiry, S.; Kakkar, R. *Chem. Phys. Lett.* **1981**, *78*, 379.
(28) Hurley, M.; Gerstein, B. C. *J. Chem. Phys.* **1973**, *59*, 6667.
(29) Gerstein, B. C.; Gehring, F. D.; Willett, R. D. *J. Appl. Phys.* **1972**, *43*, 1932.
(30) Watson, B. C. Ph.D. Thesis, University of Florida, Gainesville, FL, 2000.
(31) Ajiro, Y.; Takeo, K.; Inagaki, Y.; Asano, T.; Shimogai, A.; Mito, M.; Kawae, T.; Takeda, K.; Sakon, T.; Nojiri, H.; Motokawa, M. *Physica B* **2003**, *329*, 1008.
(32) Inagaki, Y.; Kobayashi, A.; Asano, T.; Sakon, T.; Kitagawa, H.; Motokawa, M.; Ajiro, Y. *J. Phys. Soc. Jpn.* **2005**, *74*, 2683.
(33) Yoshida, Y.; Wada, O.; Inagaki, Y.; Asano, T.; Takeo, K.; Kawae, T.; Takeda, K.; Ajiro, Y. *J. Phys. Soc. Jpn.* **2005**, *74*, 2917.
(34) Stone, M. B.; Tian, W.; Murphy, T. P.; Nagler, S. E.; Mandrus, D. G. *Am. Inst. Phys. Conf. Proc.* **2006**, *850*, 1015.
(35) Stone, M. B.; Tian, W.; Granroth, G. E.; Lumsden, M. D.; Chung, J.-H.; Mandrus, D. G.; Nagler, S. E. *Physics B*, doi: 10.1016/j.physb.2006.05.145.

inequivalent dimers along the structural chain. Adjacent chains are coupled through nonbonding chloride−chloride contacts, and although each structural chain is identical, the interchain coupling alternates between the two different types of dimer. These chloride−chloride contacts mediate antiferromagnetic exchange, and the result is two different magnetic chains that run perpendicular to the structural chain. The abundant magnetic data can now be interpreted in terms of this low-temperature structure that provides a clear example of how nonbonding halide−halide contacts can be the critical interaction that dictates magnetic behavior.

## Experimental Details

**Sample Preparation.** Catena(dimethylammonium-bis($\mu_2$-chloro)-chlorocuprate), $(CH_3)_2NH_2CuCl_3$, commonly referred to as DMA-$CuCl_3$, was formed by the slow evaporation of a 1:1 solution of $CuCl_2{\cdot}2H_2O$ and $(CH_3)_2NH_2Cl$ in methanol over a period of ∼2 weeks. Single-crystal samples with a mass of 50 mg, as well as several grams of powder, were synthesized. Deuterated single crystalline and powder samples were prepared in a similar manner by starting with $(CD_3)_2NH_2Cl$ and $CuCl_2{\cdot}2D_2O$ in deuterated methanol, where the remaining ammonium protons exchange with the deuterated solvent. For both types of samples, the resultant specimens appear reddish brown in color, and single crystal samples have a flat irregular shape that is roughly rectangular.

**X-ray Diffraction.** A suitable crystal was attached to a glass fiber. Data were collected at 295(2) K for room-temperature data and 84(2) K in a nitrogen stream[36] using a Bruker/Siemens SMART APEX instrument (Mo Kα radiation, $\lambda = 0.71073$ Å) equipped with a Cryocool NeverIce low-temperature device. Data were measured using $\omega$ scans of 0.3° per frame for 5 and 10 s, and a full sphere of data was collected. A total of 2132 frames was collected with a final resolution of 0.83 Å. The first 50 frames were recollected at the end of data collection to monitor for decay. Cell parameters were retrieved using SMART[37] software and refined using SAINTPlus[38] on all observed reflections. Data reduction and correction for Lp and decay were performed using the SAINTPlus software. The data collected at 84 K were rotationally twinned and were deconvoluted using CELL_NOW[39] giving a two-component twin with a 179.8° rotation about the reciprocal axis 1.000, 0.501, 0.505, and a twinning ratio of 0.519(1). The matrix used to relate both orientations is

0.953, 0.022, 0.071,
0.978, −0.989, 0.039,
0.987, 0.007, −0.964.

Absorption corrections were applied using SADABS (295 K data) and TWINABS (84 K data).[40] The structures were solved by direct methods and refined by least squares on $F^2$ using the SHELXTL program package.[41] All non-hydrogen atoms were refined anisotropically. No decomposition was observed during data collection. Details of the data collection and refinement are given in Table 1. Further details are provided in the Supporting Information. Crystallographic data in the form of CIF files have been deposited in the Cambridge Data Base for both the room-temperature [CCDC 299849] and low-temperature [CCDC 299850] forms.

**Table 1.** Crystal Data and Structure Refinement Parameters

| empirical formula | $C_4H_{16}Cl_6Cu_2N_2$ | $C_4H_{16}Cl_6Cu_2N_2$ |
|---|---|---|
| fw | 431.97 | 431.97 |
| $T$ (K) | 294(2) | 84(2) |
| $\lambda$(Å) | 0.71073 | 0.71073 |
| cryst syst | monoclinic | triclinic |
| space group | $C2/c$ | $P\bar{1}$ |
| $a$ (Å) | 17.445(2) | 8.478(2) |
| $b$ (Å) | 8.626(1) | 9.572(1) |
| $c$ (Å) | 11.973(2) | 10.487(2) |
| α(deg) | 90 | 73.46(2) |
| $\beta$(deg) | 125.411(2) | 68.591(7) |
| $\gamma$(deg) | 90 | 64.762(7) |
| $V$ (Å$^3$) | 1468.4(3) | 708.2(2) |
| $Z$ | 4 | 2 |
| $\rho_{calcd}$ (Mg/m$^3$) | 1.954 | 2.026 |
| $\mu$(mm$^{-1}$) | 3.956 | 4.101 |
| $F$(000) | 428 | 428 |
| independent reflns | 2050 [$R$(int) = 0.0223] | 8011 [$R$(int) = 0.0000] |
| max/min. transm | 0.727/0.429 | 0.754/0.461 |
| GOF | 1.039 | 1.056 |
| R1[a] [$I > 2\sigma(I)$] | 0.0353 | 0.0331 |
| wR2[b] [$I > 2\sigma(I)$] | 0.0917 | 0.1201 |

[a] $R1 = \sum||F_o| - |F_c||/\sum|F_o|$. [b] $wR2 = \sum w||F_o|^2 - |F_c|^2|/\sum w|F_o|^2$.

**Neutron Scattering Studies.** Neutron powder diffraction experiments were performed at the Oak Ridge National Laboratory High Flux Isotope Reactor (HFIR) and utilized the HB-3 triple axis spectrometer and a wavelength of $\lambda = 1.77874$ Å. The sample was ∼1 g of randomly arranged, deuterated microcrystals and was held in aluminum foil anchored to a support that also served as a thermal resevoir. Temperature control between 10 K and room temperature was accomplished by varying the pumping speed on an in-house $^4$He cryogenic system.

**Capacitance Measurements.** Simple parallel plate capacitance measurements were made using nominally 32 mg samples that were placed between the two parallel plates. The sample cell was designed for use with a homemade cryogenic probe capable of operating between 1.5 and 300 K. Standard null-detection bridge and low-frequency (1353 Hz) lock-in amplifier techniques were used. Liquid nitrogen or helium was used to cool to the lowest temperature, and data were acquired while slowly warming.

**Vibrating Sample Magnetometer.** High field ($0 < H < 30$ T) magnetization experiments were performed at the National High Magnetic Field Laboratory (NHMFL) in Tallahassee. These measurements used a 30 T, 33 mm bore resistive magnet and a vibrating sample magnetometer (VSM). The samples consisted of randomly oriented microcrystals that were packed into a gelcap that was held in place at the end of a fiberglass rod with Kapton tape. The VSM used a pair of counter wound pick-up coils (3500 turns/each, AWG 50). The sample was vibrated at 82 Hz. Absolute signal calibration was not necessary during our measurements because we were able to reach saturation magnetization. In addition, at saturation, we were also able to measure and subtract a small linear correction with negative slope that corresponds to the diamagnetic contribution from the gelcap, as well as the diamagnetism from the sample. The VSM has a resolution of $10^{-3}$ emu and a maximum signal of $\sim 10^4$ emu. The largest sample signal was at least an order of magnitude below this limit at 30 T, so the VSM pick-up coil response remained in the linear regime. The sample signal was greater than the minimum signal resolution of $10^{-3}$ emu at a magnetic field of ∼1 T. Temperature control was achieved by varying the pumping speed of a $^4$He bath.

(36) Hope, H. *Prog Inorg. Chem.* **1994**, *33*, 1.
(37) *SMART: Bruker Molecular Analysis Tool v.5.626*; Bruker AXS: Madison, WI, 2002.
(38) *SAINTPlus: Data Reduction and Correction Program v.6.36a*; Bruker AXS: Madison, WI, 2001.
(39) Sheldrick, G. M. *CELL_NOW*; Bruker AXS: Madison, WI, 2002.
(40) Sheldrick, G. M. *TWINABS: An Empirical Absorption Correction Program v.1.02*; Bruker AXS: Madison, WI, 2002.
(41) Sheldrick, G. M. *SHELXTL: Structure Determination Software Suite v.6.10*; Bruker-AXS: Madison, WI, 2001.

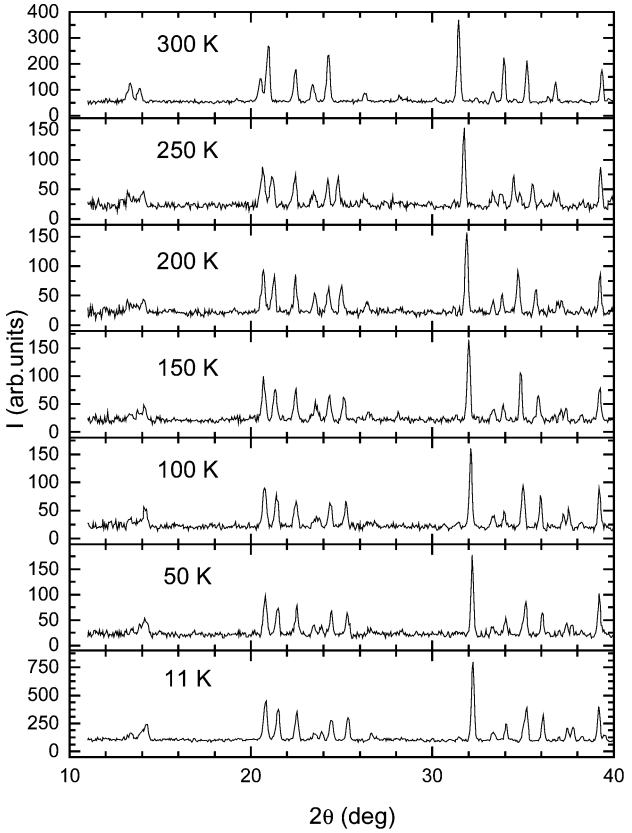


**Figure 1.** Intensities of the powder diffraction experiment are shown as a function of $2\theta$ and temperature. When cooling from 300 to 250 K, the peaks near 21° and 33° split. Additional changes are observed between 100 and 150 K, but no additional evolution of the spectra was observed between 11 and 50 K. The sample consisted of 1.1 g of randomly oriented deuterated microcrystals. Complete scans up to $2\theta = 80°$ are included in the Supporting Information.

## Results and Discussion

**Structural Phase Transition.** The structural transition is seen in powder neutron diffraction. Figure 1 shows diffraction patterns from ~1.1 g of deuterated $DMACuCl_3$ powder. The data obtained at 300 K could be indexed to the published room-temperature structure. The structural change is observed when cooling from 300 to 250 K, as the peaks near $2\theta = 21°$ and 33° split. The data are consistent with lowering of the symmetry from a monoclinic space group $I2/a$, to the triclinic space group $P\bar{1}$ (vide infra), although the detailed crystal structure of the low-temperature phase could not be resolved from the neutron data. The absence of additional intensity in any Bragg peaks as a function of temperature to $T = 11$ K indicates no evidence of long-range magnetic order. The additional peaks are only consistent with the structural transition and not magnetic order.

Low-frequency (1353 Hz) capacitance measurements were used to identify the transition temperature. Data from a powder sample sandwiched between parallel plates are shown in Figure 2. Changes in capacitance reflect changes in the dielectric constant, and the measurement provides a sensitive probe of solid-state structural changes.[42] The deviation from the room-temperature capacitance shows cusps at 286.2 K upon cooling and at 288.8 K upon warming, the hysteresis is a signature of a cooperative event that is coupled to the lattice. The location of the transition was reproducible in subsequent thermal cycles, but the signatures became weaker with successive measurements.

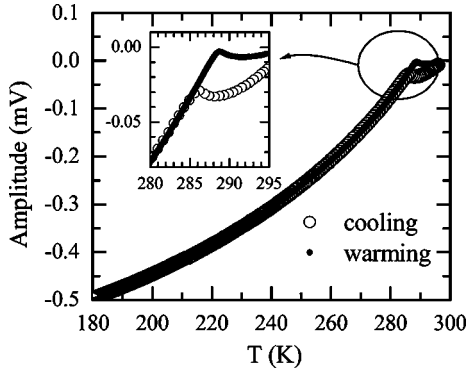


**Figure 2.** Temperature dependence of the amplitude of the capacitance change is shown as a function of temperature. The deviation from the room-temperature capacitance shows cusps at 286.2 K upon cooling and at 288.8 K upon warming. The amplitude of the in-phase signal is measured from a two-phase lock-in amplifier.

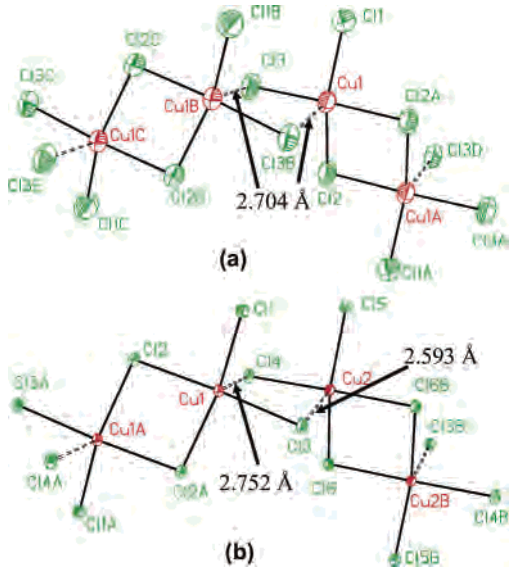


**Figure 3.** Illustration of the $Cu_2Cl_6^{2-}$ dimer chains in (a) the high-temperature phase and (b) the low-temperature phase. The semi-coordinate bonds are shown as open dashed lines. Symmetry codes: (a) $A = -x, 1 - y, 1 - z$; $B = -x, y, {}^1/_2 - z$; $C = x, 1 - y, -{}^1/_2 + z$; $D = x, 1 - y, {}^1/_2 + z$; $E = -x, 1 - y, -z$; (b) $A = 2 - x, -y, 2 - z$; $B = 2 - x, 1 - y, 1 - z$.

**Structure Descriptions.** The results of the X-ray structure determination are shown in Figures 3−6, which display the differences between the room-temperature (300 K) and low-temperature (84 K) structures.[43] The structures of both phases contain kinked chains of $Cu_2Cl_6^{2-}$ dimers. The most obvious difference between the structures of the two phases (Figure

(42) Hall, J. W.; Marsh, W. E.; Weller, R. R.; Hatfield, W. E. *Inorg. Chem.* **1981**, *20*, 1033.

(43) The structure of the centered monoclinic lattice of the room temperature was solved in the conventional $C2/c$ space group setting, in contrast to the $I2/a$ setting in the original structure report[26] (but in agreement with a later determination (Eckardt, K., Svoboda, I., Pabst, I. *Z. Kristallogr.* **1993**, *208*, 253)). The transformation matrix for the $I2/a$ lattice to the $C2/c$ lattice is [−1, 0, −1; 0, 1, 0; 1, 0, 0]. The low-temperature phase was solved in the triclinic space group $P1$. The transformation from the triclinic lattice to the $C$-centered monoclinic lattice is given by the matrix [1, −2, 0; −1, 0, 0; 0, 1, −1].

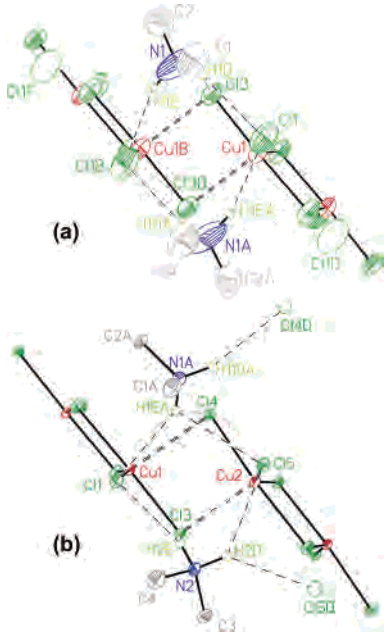


**Figure 4.** Illustration of hydrogen bonding in (a) the high-temperature phase and (b) the low-temperature phase, showing the differences in orientation of the $DMA^+$ cations in the two phases. Primary hydrogen bonds are shown as dashed lines, secondary N−H···Cl interactions by the dotted lines. Chlorine atoms from adjacent chains are shown as open ellipsoids. Symmetry codes: (a) A = B = $-x$, $y$, $^1/_2 - z$; D = $-x$, $2 - y$, $1 - z$; F = $x$, $2 - y$, $-^1/_2 + z$; (b) A = $2 - x$, $-y$, $2 - z$; B = $2 - x$, $1 - y$, $1 - z$; Cl4D = $2 - x$, $-y$, $1 - z$; Cl5D = $1 - x$, $1 - y$, $1 - z$.

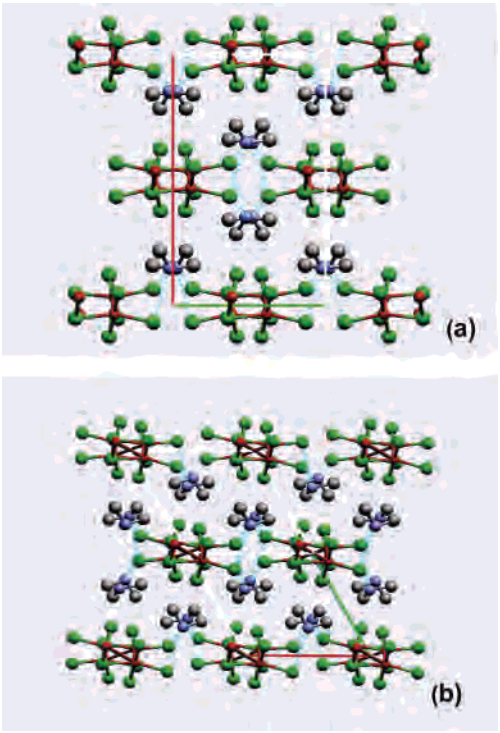


**Figure 5.** Illustration of the packing of the hydrogen-bonded layers of dimer chains. (a) room temperature (b) low temperature. Hydrogen bonds are shown as dashed lines.

4) is the mode of hydrogen bonding between the $DMA^+$ cations and the dimer chains, which induces changes both within and between the chains. The hydrogen-bonding interactions play two significant roles in the structures: (a) influencing the geometrical nature of the dimer chains (Figure

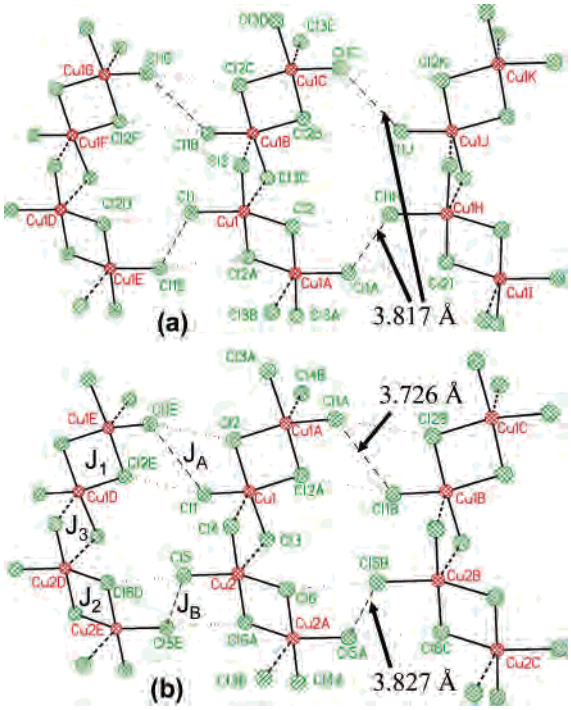


**Figure 6.** Illustration of Cl···Cl contacts between dimers (a) the high-temperature phase and (b) the low-temperature phase. In the high-temperature phase, the Cl···Cl contacts linking the dimers are equivalent. In the low-temperature phase, the Cl···Cl contacts between type 1 dimers differ from the contacts between type 2 dimers. This arrangement leads to possible exchange interactions within the structural chain, labeled $J_1$, $J_2$, $J_3$ and between structural chains, $J_A$ and $J_B$.

3) and (b) tying the chains together into a layer structure (Figure 5). The phase transition induces two particularly significant changes in the structure. First, the low-temperature dimer chains contain alternating pairs of inequivalent dimers, in contrast to the uniform dimer chains in the room-temperature phase. Second, the intralayer Cl···Cl contacts between chains reflect this change in chain structures, with the low-temperature phase showing two distinct types of Cl···Cl contacts (Figure 6). These structural differences are crucial to the understanding of the low-temperature magnetic properties of the system.

**Structural Chains.** Dimers in the chains of both compounds are linked by pairs of semi-coordinate Cu···Cl bonds to yield the common folded 4 + 1 coordination geometry for five-coordinate copper ions. The basic features of the chain structure are very similar in the two phases, as seen by the illustrations in Figure 3. The chains in both phases are composed of centrosymmetric $Cu_2Cl_6^{2-}$ dimers linked by pairs of semi-coordinate Cu···Cl bonds. Nevertheless, significant differences are seen. In the room-temperature phase, adjacent dimers are related by $C_2$ symmetry operations and all dimers (and chains) are structurally equivalent. These $C_2$ symmetry elements are lost in the low-temperature phase, and the chains contain alternating pairs of centrosymmetric dimers. The dimers themselves show the so-called bifold or sedia conformation, where the nonbridging terminal chloride ions are displaced out of the plane of the other atoms in the dimer, as illustrated in Scheme 1. The exchange coupling within the dimer structure has been shown to depend crucially

**Scheme 1**

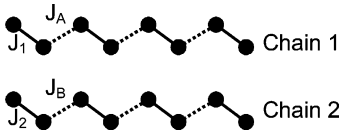


on the value of the bifold angle, $\sigma$.[4,44] From the data in Table 2, it is seen that dimer **2** of the low-temperature phase (containing Cu2) has close to the same geometry as the dimer of the room-temperature phase, with a small decrease in the bifold angle observed. The bifold angle is even smaller for dimer **1** (which contains Cu1), indicating a conformation closer to planarity. The central $Cu_2Cl_2$ bridging geometry is essentially the same for all of the dimers, with only the Cu1−Cl2A distance showing an unexpected shortening in the low-temperature phase. Another major change that occurs between the two phases in the chain structures is in the nature of the semi-coordinate linkages. With the loss of the 2-fold rotation axes, two distinct Cu···Cl semi-coordinate bonds link adjacent dimers, one shorter that that observed in the room-temperature phase and one longer.

**Hydrogen Bonding Interactions.** Pairs of cations are hydrogen bonded to the chains, as illustrated in Figure 4. This induces the kinks that are observed in the chains. The various hydrogen-bonding contacts are tabulated in Table 3. In the room-temperature phase, the pair of cations is related by a $C_2$ axis, and each one has its major hydrogen-bonding interactions with terminal chloride ions on adjacent dimers (labeled Cl1 and Cl1B in Figure 4a), with weaker interactions with chloride ions on adjacent chains (Cl1D and Cl1F in Figure 4a). In the low-temperature phases, the loss of the $C_2$ axis leads to two independent cations. Both cations are rotated so as to have their strongest hydrogen-bonding interactions with the same terminal chloride ion (labeled Cl1 in Figure 4b) and with a chloride from an adjacent chain (Cl4D and Cl5D, respectively). In the room-temperature phase, there is evidence of disorder in the hydrogen-bonding interactions, based on the shape of the thermal displacement ellipsoids for N1 and Cl1. Comparison with Figure 4b would clearly suggest that the cations in the room-temperature phase are disordered (certainly dynamically) over the two independent hydrogen-bonding arrangements present in the low-temperature phase.

**Interchain Contacts.** The effect of these hydrogen-bonding interactions is to link the chains together into a sheetlike structure, as shown in Figure 5. This forces short Cl···Cl contacts between the chains, as documented in Table 3. It is the exchange coupling through these nonbonded contacts that are crucial to the understanding of the magnetic behavior of this system. These contacts are shown in Figure 6 for the two phases, with the shortest contacts shown as dashed lines and longer contacts represented by dotted lines. In both phases, all chains are structurally equivalent and, in addition, adjacent chains in the layers are translationally equivalent. In the room-temperature phase, all Cl···Cl contacts are equivalent. However, the distortions present in the low-temperature structure lead to the formation of two different Cl···Cl contact chains: chain 1 forms from type 1 dimers, and chain 2 forms from type 2 dimers. The contact distances in the two types of chains differ by ∼0.1 Å, a difference that should be reflected in the exchange coupling via those two pathways.

**Magnetic Exchange Pathways.** The possible magnetic exchange pathways in the low-temperature structure include intradimer and interdimer coupling via halide bridges along the structural chain (*c* axis) and interdimer interactions perpendicular to the chain (along the *a* axis) mediated by chloride−chloride contacts. The different Cu−Cu exchange interactions are labeled in Figure 6b, for which constants $J_1$ and $J_2$ correspond to the intradimer Cu1−Cu1 and Cu2−Cu2 exchange along the *c* axis, and $J_3$ corresponds to interdimer Cu1−Cu2 exchange along this axis via the chloride that makes the semicoordinate bond. Exchange constant $J_A$ corresponds to coupling between Cu1 dimers along the *a* axis, and the analogous interaction between Cu2 dimers is $J_B$. Depending on the signs and relative strengths of these interactions, the possible behaviors range from isolated dimers to a two-dimensional layered network, with possibilities between these limits that include linear chains along either the *a* or *c* directions. The possibilities can be limited by examining the structure and correlating the bridging geometries with other characterized examples to obtain educated guesses about the sign and magnitude of the different exchange constants.

The geometry of the bifold dimers determines the sign and magnitude of intradimer exchange.[4,44] The $\mu$-chloride bridging angles in the two low-temperature dimers are similar, 95.72° for Cu1−Cl2−Cu1A and 95.41° for Cu2−Cl6−Cu2A. These bridging angles fall within a very narrow range (95.3−95.8°) observed in a series of $Cu_2Cl_6^{2-}$ dimers for which Willett and co-workers[4,44] correlated the sign and magnitude of the intradimer exchange constant with the bifold angle, $\sigma$. In this series, exchange constants range from ferromagnetic, $J/K = 30$ K for (4-benzylpiperidinium)$CuCl_3$ ($\sigma = 28.7°$) to antiferromagnetic, $J/K = -28$ K for (melaminium)$Cu_2Cl_6$ ($\sigma = 7.6°$). Antiferromagnetic coupling increases as the bifold angle decreases. Following this correlation, the value of Cu1, $\sigma = 19.6°$ indicates this interaction should be antiferromagnetic and can be estimated to be on the order of $J/K = -10$ K. On the other hand, the observed bifold angle in the dimer of Cu2, $\sigma = 21.7$ suggests a weak ferromagnetic exchange, although close to the value where the exchange coupling crosses over from antiferromagnetic to ferromagnetic.

The interdimer interaction, $J_3$, is via the long semi-coordinate bond and can be assumed to be near zero. In past analyses of the magnetic properties of several Cu halide dimers, modest magnetic exchange interactions were generally associated with these semi-coordinate bonds between dimers. However, it is more likely that they should be have been attributed to halide−halide contacts (vide infra). Fortunately, systems with similar types of semi-coordinate linkages have been studied in which no halide−halide contacts exist. The complex $(Et_2Me_2N)_3Cu_4Cl_{11}$ contains

(44) Scott, B.; Willett, R. D. *Inorg. Chim. Acta* **1988**, *141*, 193.

**Table 2.** Pertinent Distances (Å) and Angles (deg)

| RT phase | | LT phase − dimer 1 | | Lt phase − dimer 2 | |
|---|---|---|---|---|---|
| Cu1−Cl1 | 2.2553(9) | Cu1−Cl1 | 2.2391(10) | Cu2−Cl5 | 2.2574(9) |
| Cu1−Cl2 | 2.3056(8) | Cu1−Cl2 | 2.3151(9) | Cu2−Cl6 | 2.3123(10) |
| Cu1−Cl2A | 2.3169(7) | Cu1−Cl2A | 2.2785(10) | Cu2−Cl6c | 2.3278(9) |
| Cu1−Cl3 | 2.2753(7) | Cu1−Cl3 | 2.2818(9) | Cu2−Cl4 | 2.2962(9) |
| Cu1···Cl3B | 2.7035(9) | Cu1···Cl4 | 2.7524(9) | Cu2···Cl3 | 2.5931(9) |
| *d*(Cl1)[b] | 0.89 | *d*(Cl1) | 0.78 | *d*(Cl5) | 0.84 |
| Cl1−Cu1−Cl2 | 155.47(4) | Cl1−Cu1−Cl2A | 158.97(3) | Cl5−Cu2−Cl6 | 155.59(3) |
| Cl3−Cu1−Cl2A | 176.47(3) | Cl2−Cu1−Cl3 | 176.89(3) | Cl4−Cu2−Cl6C | 174.94(3) |
| Cu1−Cl2−Cu1A | 95.49(3) | Cu1−Cl2−Cu1a | 95.72(3) | Cu2−Cl6−Cu2A | 95.41(3) |
| Cu1···Cl3B−Cu1B[c] | 89.75(3) | Cu1···Cl4−Cu2 | 88.11(3) | Cu2···Cl3−Cu1 | 92.42(3) |
| $\sigma$[d] | 22.8 | $\sigma$ | 19.6 | $\sigma$ | 21.7 |
| Cl1···Cl1E | 3.817 | Cl1···Cl1D | 3.726 | Cl5···Cl5B | 3.827 |
| Cu1−Cl1···Cl1E | 118.8 | Cu1−Cl1···Cl1D | 119.2 | Cu2−Cl1···Cl1B | 114.4 |
| Cl1···Cl2D | 4.255 | Cl1···Cl2E | 4.182 | Cl5···Cl6D | 4.109 |
| Cu1−Cl1···Cl2D | 164.1 | Cu1−Cl1···Cl2E | 166.6 | Cu2−Cl5···Cl6D | 158.2 |
| Cu1D−Cl2D···Cl1 | 156.4 | Cu1E−Cl2E···Cl1 | 149.6 | Cu2D−Cl6D···Cl5 | 159.8 |

[a] See figures for atom labeling. [b] The distance of the named atom from the plane of the central bibridged $Cu_2Cl_2$ unit of the dimer. [c] Cu1B is the copper atom in the adjacent dimer bonded to Cl3B. [d] The dihedral angle between the central bibridged $Cu_2Cl_2$ unit and the terminal $CuCl_2$ group.

**Table 3.** Hydrogen Bonding Parameters

| atoms | N···Cl (Å) | H···Cl (Å) | N−H···Cl (deg) |
|---|---|---|---|
| RT Phase | | | |
| N1−H1D···Cl1 | 3.227 | 2.450 | 144.6 |
| *N1−H1D···Cl3* | *3.575* | *2.911* | *131.8* |
| N1−H1E···Cl1B | 3.254 | 2.435 | 151.4 |
| *N1−H1E···Cl1F** | *3.576* | *3.035* | *120.4* |
| LT Phase | | | |
| N1A−H1DA···Cl4D* | 3.271 | 2.387 | 160.6 |
| *N1A−H1DA···Cl5* | *3.150* | *2.887* | *98.0* |
| N1A−H1EA···Cl1 | 3.204 | 2.432 | 141.5 |
| *N1A−H1EA···Cl4* | *3.444* | *2.916* | *118.0* |
| *N1A−H1EA···Cl5* | *3.150* | *2.675* | *112.9* |
| N2−H2DA···Cl5D* | 3.203 | 2.438 | 140.6 |
| *N2−H2DA···Cl5* | *3.261* | *2.703* | *119.9* |
| N2−H2EA···Cl1 | 3.193 | 2.317 | 148.7 |
| *N2−H2EA···Cl3* | *3.561* | *2.875* | *132.4* |
| *N2−H2EA···Cl5* | *3.261* | *2.945* | *101.9* |

[a] Refer to Figure 4 for the labeling scheme. The parameters for the weaker interactions (shown as dotted lines in Figure 2) are italicized.

ferromagnetically coupled tetramers joined by semi-coordinate linkages similar to the ones in $DMACuCl_3$, with $J'/k = -2.5$ K[45] and $(EtMe_3N)_4Cu_5Cl_{14}$ has a similar structure of ferromagnetically coupled pentamers with $J'/k = -1.5$ K.[46] The salt $(HPy)_2[Cu_3Cl_8](H_2O)_2$ contains chains of trimers, now where the exchange through the semi-coordinate linkage has a value of $J'/k = +1.9$ K.[47] In $KCuCl_3$ and $TlCuCl_3$, neutron scattering experiments have shown the semi-coordinate linkages have an exchange coupling of ~2.8 K.[48] Thus, experimentally, these semi-coordinate linkages have either ferro- or antiferromagnetic exchange coupling with exchange constant values near zero. This is not unexpected since the magnetic electrons lie in MOs that are composed of the $d_{x^2-y^2}$ orbitals on Cu ions and $p_\sigma$ orbitals on Cl ions that lie in the plane of the dimer. Since the planes of adjacent dimers are essentially parallel, the overlap of the magnetic orbitals on adjacent dimers is expected to be small, leading to small values for the exchange coupling.

The low-temperature magnetic properties, discussed further below, are not adequately explained on the basis of the structural chain of alternating dimers. Additional interactions are required. Recent neutron scattering results indicate the presence of one-dimensional coupling in the direction perpendicular to the structural chain.[35] In this direction, only nonbonding chloride−chloride contacts link adjacent dimers. Nonetheless, nonbonding chloride−chloride contacts can provide an important magnetic exchange pathway.[3,5,12,17−20,22,23,25] Halide−halide contacts (two-halide exchange) were shown to be responsible for interlayer antiferromagnetic exchange in some members of the family of layered compounds, $[H_3N(CH_2)_nNH_3]CuCl_4$ and $[H_3N(CH_2)_n$-$NH_3]CuBr_4$.[17−20] The important interlayer metric was shown to be the halide−halide distance, not the distance between metal ions.[19] Furthermore, two-halide exchange via Br···Br contacts is observed to be stronger than through Cl···Cl contacts.[18,25] Such contacts have now been observed to influence magnetic properties in other systems, and the importance of this interaction is the subject of a recent review.[25]

Many variables can influence the sign and strength of magnetic exchange through two-halide bridges.[25] However, it is qualitatively accepted that, for similar metal coordination geometries, the strength of the magnetic exchange via nonbonded Cu−X···X−Cu pathways should increase as the Cu−X···X angle becomes larger and as the X···X distance becomes shorter.[22,23] In fact, an exponential dependence of halogen−halogen distance on exchange constant has previously been noted.[18,25]

The two-halide bridges that link the two types of dimers into chains are different. The Cl···Cl distance of chain 1 (linking dimers of Cu1) is 3.726 Å, and the Cu−Cl··Cl angle is 119°, whereas the analogous distance and angle for chain 2 are 3.827 Å and 114°, respectively. Both interactions are antiferromagnetic, but the shorter distance and larger angle for the two-halide bridge of chain 1 indicates that $|J_A| > |J_B|$.

(45) Fujii, Y.; Wang, Z.; Willett, R. D.; Zhang, W.; Landee, C. P. *Inorg. Chem.* **1995**, *34*, 2870.
(46) Bond, M. R.; Willett, R. D.; Rubenacker, G. V. *Inorg. Chem.* **1990**, *29*, 2713.
(47) Bhattacharya, R.; Ghosh, A.; Ray, M. S.; Righi, L.; Bocelli, G.; Chaudhuri, S.; Willett, R. D.; Clemente-Juan, J. M.; Coronado, E.; Gomez-Garcia, C. J. *Eur. J. Inorg. Chem.* **2003**, 4253.
(48) Matsumoto, M.; Normand, B.; Rice, T. M.; Sigrist, M. *Phys. Rev. B* **2004**, *69*.

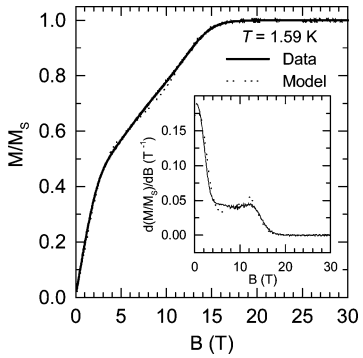


**Figure 7.** Magnetization of a 200.8 mg sample of randomly oriented microcrystals is shown as a function of magnetic field at 1.59 K. The signal is normalized to the saturation magnetization. A small diamagnetic linear dependence was subtracted from the data, $\chi_{dia} = -1.196 \times 10^{-3}$ emu/mol. At 1.59 K, the magnetization has two distinct first derivative changes at approximately 3 and 16 T, with approximately linear behavior between those points.

Following this structural analysis, a magnetic model for $DMACuCl_3$ can be proposed that consists of two independent chains that run along the *a* axis, Scheme 1. Chain 1, comprised of Cu1 ions, is an alternating chain with two exchange constants, $J_1$ and $J_A$. Both values are likely antiferromagnetic. Chain 2 can be described as ferromagnetically coupled Cu2 ions linked weakly by the antiferromagnetic interaction $J_B$. This model is consistent with previously published magnetic observations that include at least one ferromagnetic dimer interaction[4,44] and low-dimensional antiferromagnetic exchange evident at low temperature.[29] The two-chain model is also consistent with the observations of Yoshida et al.[33] that more than two exchange interactions are required and the neutron scattering results of Stone[35] and co-workers that quasi one-dimensional coupling propagates in the direction of the Cu−Cl···Cl−Cu contacts.

**High-Field Magnetization.** To illustrate the plausibility of this analysis, we applied the two-chain model of Scheme 1 to the unusual low-temperature magnetization vs field behavior $DMACuCl_3$. The results of our own high-field ($0\ T < H < 30\ T$) magnetization studies are shown in Figure 7. At 1.59 K, the magnetization has two distinct first derivative changes near 3 and 16 T, with approximately linear behavior between those points (see inset of Figure 7). This behavior is not particular to this sample, and the kink at 3.2 T was observed in studies performed up to 5 T while at 2 K.[30] Our results are strikingly similar to the data report by O'Brien and co-workers[4] and are consistent with the results obtain by Inagaki and co-workers at different temperatures.[32,33]

From the magneto-structural considerations of the low-temperature phase, the system can be modeled as two, $S = 1/2$ magnetic chains that are noninteracting if $J_3$ is negligible. Specifically, the Hamiltonian of chain 1 is

$$H_1 = -J_1 \sum_{i=1}^{N/2} S_{2i-1}S_{2i} - J_A \sum_{i=1}^{N/2-1} S_{2i}S_{2i+1} + g\mu_B B \sum_{i=1}^{N} S_i^z \quad (1)$$

which is often referred to as an alternating bond chain,[49−51] and the Hamiltonian of chain 2 is

$$H_2 = -J_2 \sum_{i=1}^{N/2} S_{2i-1}S_{2i} - J_B \sum_{i=1}^{N/2-1} S_{2i}S_{2i+1} + g\mu_B B \sum_{i=1}^{N} S_i^z \quad (2)$$

where $g$ is the Lande factor, $\mu_B$ is the Bohr magneton, and $B$ is the external magnetic field. In the limit that the $J_2$ dimers are strongly ferromagnetically coupled to form effective $S = 1$ spins, then chain 2 becomes a Haldane chain[52,53] whose finite temperature magnetization has been studied numerically.[54,55]

To calculate $M$ ($B$, $T = 1.59$ K) for each chain, exact diagonalization methods were employed for $N = 12$.[30,56] The measured $g$ value is anisotropic, and an average of $g = 2.1$ was used in the calculation.[30] The results of the calculation are shown in Figure 7, where $J_1 = -10$ K, $J_A = -8$ K, $J_2 = 18$ K, and $J_B = -2.5$ K. In other words, $J_2$ is the only ferromagnetic interaction while the remaining couplings are antiferromagnetic. Of course, the magneto-structural considerations allow us to assign specific values to $J_2$ and $J_B$; however, the values assigned to $J_1$ and $J_A$ are not uniquely determined, i.e., they could be interchanged without altering the results of the numerical work. The calculation reasonably reproduces the trends of the data, and deviations from the fit occur when any $J$ parameter, except $J_2$, varies by approximately ±1 K. The fit is less sensitive to the magnitude of $J_2$. On the other hand, the data cannot be fit by different choices of the signs of the interactions. The calculated response reasonably reproduces the experimental data, demonstrating the plausibility of the two independent chain model for the system. The calculation suggests the presence of additional features that are not resolved in our data but may be evident the lower-temperature data of Inagaki et al.[32] Measurement of the magnetic response of oriented crystals instead of the random arrangement used in our measurement could be helpful in this regard. Furthermore, a complete model should include a finite interchain coupling, $J_3$, which presumably drives the transition to long-range order that was observed below 1 K.[31]

It is important to stress that, due to the restricted spin size of $N = 12$, the exact diagonalization of the proposed Hamiltonians, eqs 1 and 2, is not expected to provide definitive values for the parameters when the temperature is less than any $J$ value.[30] Furthermore, the set of parameter values are not uniquely determined by simple fitting of the data. For example, if $J_1$, $J_A$, and $J_3$ are assumed to be zero, i.e., the spins in chain 1 behave as noninteracting free spins,

(49) Lynden-Bell, R. M.; McConnell, H. M. *J. Chem. Phys.* **1962**, *37*, 794.
(50) Duffy, W., Jr.; Barr, K. P. *Phys. Rev.* **1968**, *165*, 165.
(51) Bonner, J. C.; Friedberg, S. A.; Kobayashi, H.; Meier, D. L.; Blote, H. W. J. *Phys. Rev. B* **1983**, *27*, 248.
(52) Affleck, I. *J. Phys. Condens. Matter* **1989**, *1*, 3047.
(53) Yamashita, M.; Ishii, T.; Matsuzaka, H. *Coord. Chem. Rev.* **2000**, *198*, 347.
(54) Yamamoto, S.; Miyashita, S. *Phys. Rev. B* **1995**, *51*, 3649.
(55) Delica, T.; Kopinga, K.; Leschke, H.; Mon, K. K. *Europhys. Lett.* **1991**, *15*, 55.
(56) Weller, R. Ph.D. Thesis, University of North Carolina, Chapel Hill, NC, 1980.

then a fit similar to the one shown in Figure 7 is obtained for antiferromagnetic $J_2$ and $J_B$ values.[30] On the basis of our magneto-structural arguments, we consider this alternative microscopic description to be unphysical. In fact, preliminary analysis of inelastic neutron scattering results[35] suggests that $J_2$ is ferromagnetic, $J_B$ is antiferromagnetic, and the ratio $|J_B|/|J_2| \approx 0.9$, while the remaining possible $J$ couplings are potentially negligibly small. In this limit, our numerical fitting of the magnetization data are not expected to give quantitative results, but the qualitative nature of ferromagnetic $J_2$ and antiferromagnetic $J_B$ interactions are consistent with this possible description. Ultimately, the strength of the magnetic interactions will eventually emerge when a full analysis of the inelastic neutron scattering results are completed.

## Conclusions

The room-temperature crystal structure of $DMACuCl_3$ consisting of a linear chain of $Cu^{2+}$ dimers cannot account for the unusual magnetic properties that have been reported. A transition observed below room temperature by neutron scattering and capacitance measurements leads to a different low-temperature phase that consists of two independent magnetic chains, one an alternating antiferromagnetic chain of $Cu^{2+}$ ions and the other an antiferromagnetic chain of $S = 1$ copper dimers. X-ray structure determination at 84 K shows that resolution of disorder in the counterion network leads to two different structural dimers. Chloride−chloride contacts between structural chains that are uniform at high temperature also change at low temperature, leading to the two different magnetic chains. Importantly, magnetic exchange via the nonbonding choride−chloride contacts are critical for interpreting the magnetic data. The finite temperature magnetization arising from two magnetic spin chains can reproduce the magnetization vs field data, demonstrating the plausibility of the model. This description is consistent with recent inelastic neutron scattering experiments.[35]

**Acknowledgment.** The Bruker (Siemens) SMART APEX diffraction facility was established at the University of Idaho with the assistance of the NSF-EPSCoR program and the M. J. Murdock Charitable Trust, Vancouver, WA. This work was supported, in part, by the National Science Foundation through support of the NHMFL (DMR-9900855) and Grants No. DMR-0305371 (M.W.M.) and DMR-0543362 (D.R.T.). Work at Oak Ridge National Laboratory (ORNL) is sponsored by the Office of Basic Energy Sciences, U.S. Department of Energy, under Contract No. DE-AC05-00OR22725 with ORNL, managed and operated by UT-Battelle, LLC. We gratefully acknowledge early contributions from Debbie Jensen, James R. Maloney, James M. Stock, and Sara J. Gamble. We thank Matthew B. Stone and Yuji Inagaki for communicating their results prior to publication and for enlightening conversations.

**Supporting Information Available:** Complete scans of the powder neutron data of Figure 1. This material is available free of charge via the Internet at http://pubs.acs.org.

IC060654U